Journal of Geosciences and Geomatics, 2017, Vol. 5, No. 5, 218-228
Available online at http://pubs.sciepub.com/jgg/5/5/1

DOI:10.12691/jgg-5-5-1

Geochemical Characterization of a Stratigraphic Log Bearing Iron Ore in the Sanaga Prospect, Upper Nyong Unit of Ntem Complex, Cameroon

Ilouga D. C. I.[1,*], Ndong Bidzang F.[2], Ziem A Bidias L. A.[1,3], Olinga J. B.[2], Tata E.[4], Minyem D.[3]

[1]Geology Laboratory, Higher Teacher Training College, University of Yaounde I de Yaoundé I, Yaoundé, Cameroun
[2]Ore Processing Laboratory, IRGM, Yaounde, Cameroon
[3]Department of Earths Sciences, University of Yaounde I, Yaounde, Cameroon
[4]Department of Geology, University of Buea, South West Region, Buea, Cameroo
*Corresponding author: ilougacharles@ yahoo.fr

Abstract The Sanaga prospect in the north of Edea is located in the upper Nyong unit of the Ntem complex in Cameroon. The objective of this study is to use geochemical data trends for major and some trace elements to constrain the origin and/or sources of various constituents in the iron-bearing units as well as assess their economic potentials. The rock samples were collected from a single drill core sampled at various depths. Major elements were analysed using X-ray fluorescence spectrometry after powder digestion following. All data were processed with the aid of XLSTAT. The stratigraphic log described revealed from top to bottom two lithological sequences composed of oxidized formations (oxidized cap and oxidized gneiss), and gneissic formations (magnetite gneiss, magnetite amphibolite gneiss and enriched magnetite amphibolite gneiss successions). Detailed examination showed that quartz and iron oxides are the main minerals present. Bulk geochemical analysis of the oxidized and gneissic formations showed that Fe_2O_3 and SiO_2 are the main constituents (averaging 84.40 wt % and 92.54 wt %, respectively), confirming that quartz and iron oxides are the major mineral phases in both the oxidised and gneissic formations. Al_2O_3 averages 9.34 wt % and 3.06 wt %, Na_2O averages 0.04 wt % and 0.59 wt %, K_2O averages 0.26 and 0.53 wt %, and P_2O_5 0.07 and 0.05 wt %, respectively, in both oxidized and gneissic formations. Concentrations of trace elements in the various lithologies are generally very low (< 100 ppm). Certain correlations of interest in both units include Al_2O_3 with LOI (r > 0.8), and Zr (r > 0.7); LOI with Zr (r > 0.8). From these data it appears that mineralisation at the Sanaga prospect is restricted to the magnetite gneiss. The high concentration of Al_2O_3 (average 9.34 wt %) in the oxidized iron formations is partially due to its introduction during recent chemical weathering. The Sanaga iron formations are metamorphosed chemical sediments formed by precipitation of iron and silica from a mixture of seawater and hydrothermal fluids with a significant terrigenous input.

Keywords: *upper Nyong, Sanaga, stratigraphic log, magnetite gneiss, hydrothermal*

Cite This Article: Ilouga D. C. I., Ndong Bidzang F., Ziem A Bidias L. A., Olinga J. B., Tata E., and Minyem D., "Geochemical Characterization of a Stratigraphic Log Bearing Iron Ore in the Sanaga Prospect, Upper Nyong Unit of Ntem Complex, Cameroon." *Journal of Geosciences and Geomatics*, vol. 5, no. 5 (2017): 218-228. doi: 10.12691/jgg-5-5-1.

1. Introduction

There has been extensive investigations on the distribution, stratigraphy and origin of the iron-formations worldwide and in Cameroon [1-12]. Most of these investigations aim at determinate the origin of iron formations in order to obtain a large data set that can justify their genetic models. Understanding the genesis of iron ore deposits has traditionally been carried out using geochemistry of either: major/trace elements, rare earth elements, fluid inclusion microthermometry, solute chemistry, stable isotopes, radiogenic isotopes, organic matter, active gas chemistry and noble gas isotopes [13-18]. Several geochemical data are present in the literature, and still many factors are detracting from analytical values as contribution to comprehensive understanding of the composition of these rocks despite all these. It is therefore still leading to inadequately knowledge on the chemical composition of iron formations. According to [19] chemical analysis of iron formations fall into three main categories: (1) a general petrographic and chemical characterization; (2) determination of ore potential; and (3) understanding of origin and evolution.

In this paper, we provide new macroscopic description and geochemical data of iron-bearing mineralisation in a stratigraphic sequence in South Cameroon with the focus on deciphering the geochemical trends for major and trace elements, which may lead to some constraints about the origin and/or sources of chemical components in the iron formations. Furthermore, the chemical composition of this iron formations are compared with others world known deposits to assess its quality and evaluate the iron potential for eventual exploitation.

2. Geological Overview

The Sanaga iron ore prospect is located at the extreme end of the Nyong unit within the Archean Ntem complex, which is at the north-western end of the Congo Craton (Figure 1). The Nyong Unit constitutes the main Paleoproterozoic unit in Cameroon [20, 21]. Deformation in the Ntem complex can be divided into two major events: (1) the Archean event marked by the successive diapiric emplacement of Mesoarchean charnockites and TTGs and (2) a Paleoproterozoic transcurrent deformation phase marked by the expansion of N-S to NE-SW trending shear zone and partial melting of the TTG and the greenstone belt [22,23]. The complex is made up of three units namely: Ayina unit, Ntem Unit and the Nyong unit were the study area belong.

The lithologies that are encountered in the Nyong unit include: metamorphosed mafic–ultramafic rocks, expressed as pyroxenites and amphibolites [24], orthogneisses and metaquartzites with a dominance of biotite–amphibole–hornblende–quartz gneiss, pyroxene–amphibole–garnet–gneiss and magnetite-bearing gneiss [25], and the main plutonic rocks made of syn- to late-tectonic charnockites, alkaline syenites and post-tectonic metadiorites [20,21].

Gneisses in the unit have undergone Pan-African rejuvenation as supported by the presence of similar rocks in the Pan-African mobile belt north of the Congo Craton [20]. The biotite-hornblende gneisses are of TTG composition [26] and are spatially related to the orthopyroxene-garnet gneisses (charnockites), garnet-amphibole, pyroxenites and BIF that have been intruded and deformed by the metagranitoids. Magnetite gneiss formations occurrence are lenticular and often appear as quartz–magnetite gneiss, biotite–quartz–magnetite gneiss, biotite–amphibole–magnetite gneiss, biotite–amphibole–magnetite-garnet gneiss and pyroxene–garnet–magnetite gneiss with a characteristic pinch and swell morphology [27].

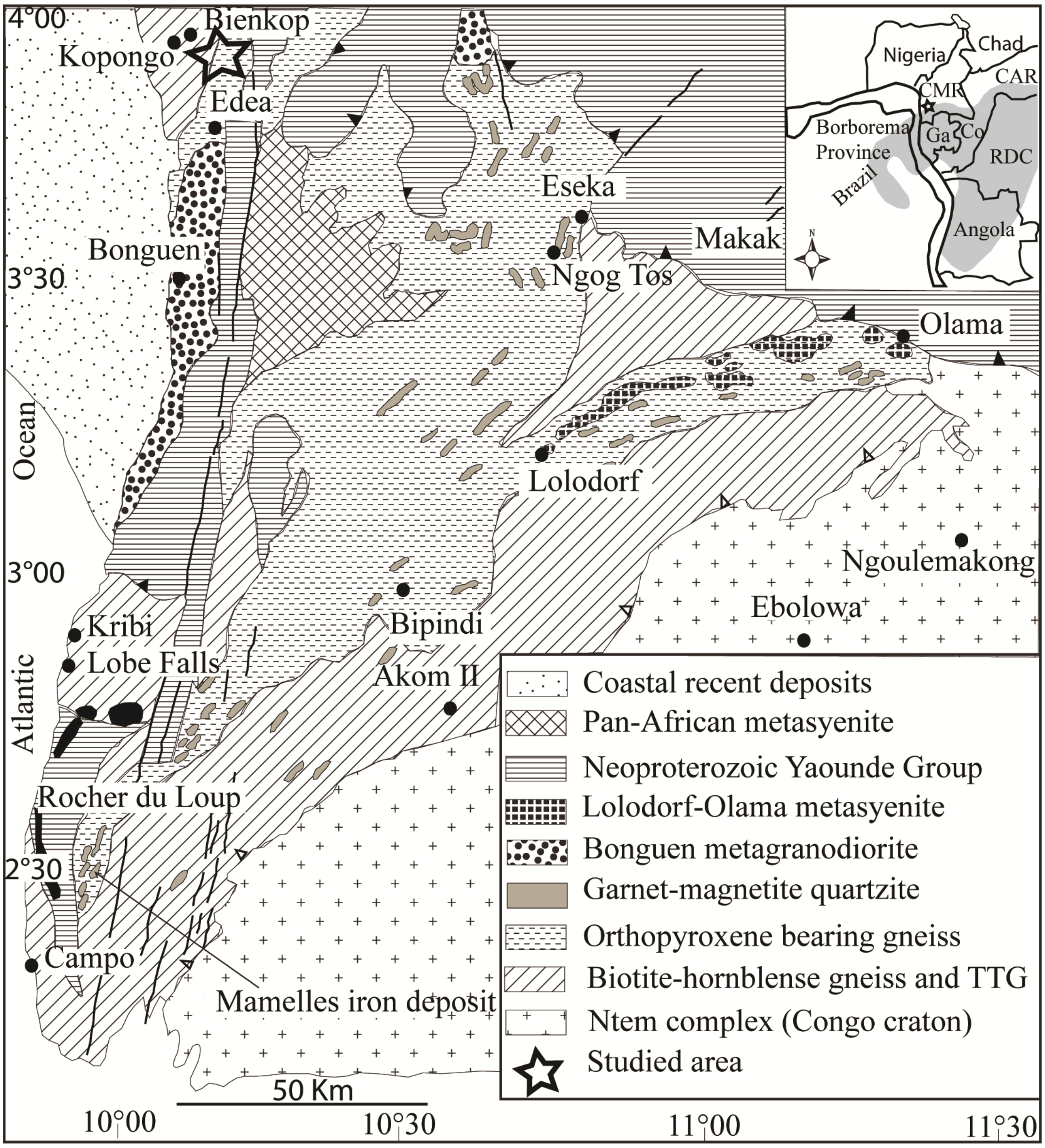

Figure 1. Geological map showing the location of the study area in the Upper Nyong Unt (from [21])

3. Sampling and Analytical Methods

Chemical sampling of one selected diamond drill hole was done following the various lithologies of iron bearing rocks and a total of 34 samples were taken. The sample core length was taken below 1m at top hole up to 33m, then above 1 m until bottom hole after this depth depending on the lithology. Samples were selected from a diamond core and halved using a core cutting machine, and then quartered at the Cameroon Mining Company (CMC). The sample preparation was completed with drying, crushing, splitting and pulverizing at ALS Laboratory in Yaoundé Cameroon. Furthermore, major and selected trace element (As, Ba, Co, Cr, Cu, Ni, P, Pb, S, V, Zn and Zr) concentration were analysed using the lithium borate fusion technique, coupled with X-ray fluorescence spectrometer with a relatively standard deviation (RSD) of 5% at the ALS laboratory of Johannesburg in South Africa. Loss on ignition (LOI) was determined by weight difference after ignition at 1000ºC. Certified reference material, duplicate and quartz blanks were randomly inserted into the sample batches as part of a continuous sample number to ensure quality assurance and quality control.

Chemical data processing was done using XLSTAT and permit to obtained line formulas, summary statistics and correlation coefficient of Patterson for the two lithological sequences.

4. Results

4.1. Macroscopic Log Description

Stratigraphic log sequence of the selected diamond hole is summarized in Table 1. The log described showed from top to bottom two lithological sequence composed of: oxidized formations (oxidized cap and oxidized gneiss), and gneissic formations (magnetite gneiss, magnetite amphibolite gneiss and enrich magnetite amphibolite gneiss successions), (Figure 2). The oxidized cap is the near surface enriched mineralization. They are located at top of the stratigraphic sequence (Figure 2 and Table 1), and composed of the oxidized cap and oxidized gneiss. The mineralogy is mainly composed of iron oxides (magnetite, goethite, and hematite), some quartz and rare clay.

The gneiss formations presented a characteristic pinch and swell morphology, and the transition between the various units is either sharp or gradational. Magnetite is the main iron oxide in the gneissic formation. The magnetite gneiss bands are sometimes observed at different stratigraphic locations with quartz lodes intruded within the gneissic assemblage. Massive magnetite vein-like features are observed toward bottom log in the magnetite gneiss formation.

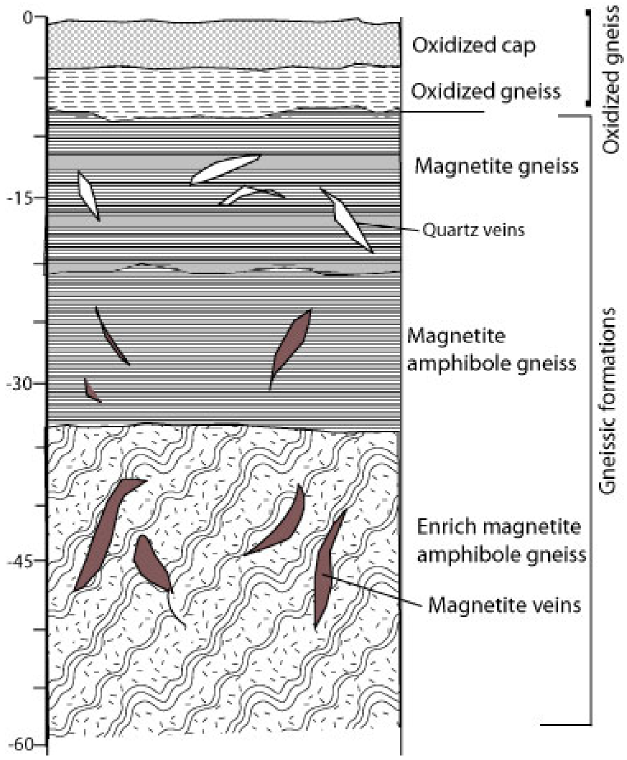

Figure 2. Stratigraphic log sequence of the described drill hole from the Sanaga prospect

4.2. Geochemistry

4.2.1. Range and Stratigraphic Variation of Major Elements

Whole-rock chemical analyses of all the facies were carried out in one diamond drill hole of 60 m depth in quarter core representing the iron bearing lithological types formed by the oxidized and the gneissic formations. From this it appear clearly that Fe and Si are the main components with 88 wt % of the rock (averaging 42.13 wt % and 45.63 wt % respectively) (Table 2).

Table 1. Stratigraphic log sequence with the characteristic of the various lithotypes

Depth (m)	Lithotypes	Mineralogy	Structures
0.80 – 4.25	Oxidised Cap	Goethite, hematite, magnetite, quartz.	foliation relic
4.25 – 8.43	Oxidised gneiss	Goethite, hematite, magnetite, quartz.	foliation
8.43 – 20.82	Magnetite gneiss	Magnetite, goethite, hematite, quartz.	foliation
20.82- 33.00	magnetite amphibole gneiss	Magnetite, quartz, amphibole, goethite.	Foliation, fracture
33.00 – 59.24	Enrich magnetite amphibole gneiss	Magnetite, quartz, amphibole, goethite.	Foliation, fracture, vein-like structures

Table 2. Major elements (wt %) geochemistry of the selected diamond drill hole in the Sanaga prospect.

Lithotypes	From	To	Sample	Al_2O_3	Fe_2O_3	SiO_2	K_2O	MgO	MnO	Na_2O	CaO	TiO_2	Cr_2O_3	P_2O_5	S	LOI	Si/Al
Oxidised cap	0.80	1.15	106703	6.57	57.19	31.20	0.04	0.05	0.03	0.01	0.01	0.37	0.01	0.06	0.03	4.35	4.75
	1.15	1.80	106704	7.51	50.74	36.00	0.04	0.04	0.03	0.01	0.02	0.44	0.01	0.09	0.04	5.53	4.79
	1.80	2.95	106705	3.51	58.18	36.60	0.02	0.03	0.03	0.01	0.01	0.22	0.01	0.04	0.03	2.37	10.43
	2.95	3.75	106706	2.16	58.54	38.80	0.01	0.02	0.03	0.05	0.01	0.09	0.01	0.03	0.02	0.56	17.96
	3.75	4.25	106708	2.83	55.77	40.40	0.00	0.02	0.03	0.05	0.01	0.18	0.00	0.04	0.02	0.38	14.28
Oxidised gneiss	4.25	5.70	106709	9.37	47.79	36.90	0.05	0.03	0.03	0.05	0.01	0.51	0.01	0.07	0.05	5.12	3.94
	5.70	6.60	106710	17.85	19.78	49.80	0.05	0.02	0.01	0.05	0.01	1.20	0.01	0.14	0.07	10.13	2.79
	6.60	7.80	106711	25.40	20.31	36.10	0.11	0.13	0.01	0.01	0.83	2.02	0.02	0.27	0.08	14.05	1.42
	7.80	8.43	106713	23.10	30.65	27.60	0.05	0.09	0.01	0.05	0.01	2.05	0.01	0.29	0.08	14.54	1.19
Magnetite gneiss	8.43	8.79	106714	6.96	50.97	36.80	0.01	0.05	0.03	0.05	0.01	0.54	0.00	0.13	0.03	4.52	5.29
	8.79	9.43	106715	1.12	56.19	42.20	0.01	0.05	0.03	0.05	0.01	0.06	0.00	0.04	0.01	0.60	37.68
	9.43	10.25	106716	1.20	57.79	40.00	0.01	0.03	0.03	0.05	0.01	0.08	0.00	0.04	0.01	0.57	33.33
	10.25	11.77	106717	1.08	53.82	42.90	0.00	0.09	0.02	0.05	0.03	0.07	0.00	0.04	0.01	0.65	39.72
	11.77	13.00	106718	2.02	52.34	44.00	0.01	0.07	0.03	0.05	0.01	0.20	0.00	0.05	0.01	1.18	21.78
	13.00	14.60	106719	1.34	53.27	43.10	0.01	0.47	0.03	0.02	0.25	0.13	0.00	0.03	0.01	0.76	32.16
	14.60	15.58	106720	11.75	27.55	54.30	0.17	0.10	0.08	0.05	0.01	0.24	0.00	0.03	0.02	5.12	4.62
	15.58	16.25	106721	18.55	6.96	65.80	0.40	0.25	0.02	0.05	0.01	0.22	0.00	0.03	0.01	7.37	3.55
	16.25	17.83	106723	16.40	17.77	57.70	0.43	0.32	0.03	0.05	0.01	0.19	0.00	0.03	0.01	6.74	3.52
	17.83	19.25	106724	16.40	7.39	65.40	2.52	0.65	0.05	0.07	0.01	0.24	0.00	0.03	0.01	6.02	3.99
Magnetite amphibole gneiss	19.25	20.82	106725	11.75	24.98	54.90	1.27	1.29	0.14	0.02	0.18	0.73	0.00	0.11	0.01	4.76	4.67
	20.82	22.25	106726	7.50	29.72	56.10	0.58	0.63	0.09	0.54	2.98	0.30	0.01	0.07	0.00	1.66	7.48
	22.25	24.00	106728	6.72	31.98	54.70	1.60	1.23	0.05	1.44	1.10	0.24	0.00	0.05	0.01	-0.05	8.14
	24.00	27.00	106731C	8.69	23.32	59.10	2.00	1.78	0.06	2.26	1.82	0.23	0.00	0.05	0.01	-0.06	6.80
	27.00	30.00	106735C	1.58	48.17	47.00	0.33	1.80	0.06	0.20	1.09	0.10	0.00	0.06	0.00	-1.05	29.75
	30.00	33.00	106738C	6.89	31.61	51.60	0.81	2.93	0.09	1.72	3.88	0.36	0.01	0.04	0.01	-0.30	7.49
Enrich magnetite amphibole gneiss	33.00	36.00	106741C	0.59	53.72	43.70	0.04	1.88	0.05	0.08	1.19	0.08	0.00	0.05	0.00	-1.39	74.07
	36.00	40.00	106746C	0.70	54.29	43.50	0.07	2.04	0.06	0.07	0.87	0.09	0.00	0.05	0.00	-1.26	62.14
	40.00	44.00	106751C	3.37	44.40	49.40	0.89	1.54	0.06	0.75	1.02	0.15	0.00	0.05	0.01	-0.77	14.66
	44.00	47.00	106755C	0.48	55.40	41.90	0.02	1.92	0.06	0.07	1.07	0.04	0.01	0.05	0.00	-1.33	87.29
	47.00	50.00	106758C	0.88	50.97	44.30	0.14	2.17	0.06	0.13	1.11	0.06	0.00	0.05	0.00	-1.37	50.34
	50.00	53.00	106761C	1.00	50.33	45.50	0.16	1.88	0.06	0.14	1.06	0.06	0.00	0.05	0.00	-1.31	45.50
	53.00	56.00	106765C	1.51	48.37	45.90	0.23	2.26	0.07	0.33	1.72	0.31	0.00	0.05	0.00	-0.97	30.40
	56.00	58.00	106768C	1.82	49.60	44.80	0.41	2.31	0.07	0.41	1.66	0.35	0.00	0.05	0.00	-1.09	24.62
	58.00	59.24	106769	1.23	52.55	43.70	0.22	2.07	0.09	0.22	1.38	0.23	0.00	0.06	0.00	-1.06	35.53

Oxidized formations

Bulk analyses indicated that Fe percentage ranges between 6.96 and 58.54 wt % (average 40.40 wt %), while silica varies between 27.60 and 65.80 wt % (average 44.02 wt %). The low Fe is due to the abundance of quartz veins cross-cutting some sections. Al_2O_3 percentage is between 1.08 and 25.40 wt % (average 9.34 wt %), while LOI varies between from 0.38 - 14.54 wt % (Table 3). The contain in this two element reduced with depth and could be indicative of the presence of clays minerals that equally reduce with depth. Again, average TiO_2 is 0.49 wt % with some value greater than 2 wt %, while phosphorous is between 0.02 – 0.28 wt % (average 0.7 wt %). A relative elevated Al and Ti contents in the sequences suggest trace input of detrital materials [28]. The alkali contents (Na_2O and K_2O) are significantly low averaging 0.04 and 0.26 wt % respectively. MgO and CaO varies between 0.02 – 1.29 wt % (average 0.19 wt %) and 0.005 – 0.83 wt % (average 0.07 wt %) respectively. The concentration of these elements increase with depth. In general, the oxidized formations are marked by low concentration of major elements apart from iron, silica and alumina. The bottom unit is marked by a slight enrichment in MgO, Na_2O and CaO.

Gneissic formations

Fe_2O_3 and SiO_2 are the main constituent (average 92.54 wt %) with values ranging between 23.32 – 55.40 wt % and 41.90 – 59.10 wt % respectively (Table 3). Al_2O_3 range between 0.48 and 8.69 wt % (average is 3.06 wt %). Na_2O and K_2O respectively range between 0.07 – 2.26 wt % and 0.01 – 2.00 wt %. Phosphorous content is very low varying from 0.04 – 0.07 wt % (average 0.05 wt %). MgO and CaO increase in the gneissic formation compared to the oxidized formations with average value of 1.89 and 1.56 wt % respectively. This enrichment in MgO and CaO with depth associated to the absence of LOI (negative values) is due to the presence of amphibole minerals and facies change. The other major elements display a very low concentration (Table 2). Again, the sharp transition between magnetite gneiss and amphibolite gneiss is marked by an increase in MgO, and CaO.

4.2.2. Range and Stratigraphic Variation of Trace Elements

The concentration of trace elements in the various lithologies is generally very low (< 100 ppm). Compared to major element chemistry that clearly differentiates each lithotypes, trace element concentrations are not as clearly indicative of a particular lithology (Table 4). Oxidized formations are more depleted in trace elements than gneissic. The latter is slightly enrich in Cl (ranging between 0.01 – 35.00 ppm), Sr, (ranging between 3.00 – 63 ppm in amphibole bearing gneiss) and Ba (ranging between 0.01 – 91.00 ppm), while the former has higher contents in Zr (ranging between 7.00 – 43 ppm) and V (ranging between 2.00 – 21.00 ppm).

Table 3. Average range of major elements analytical data of the oxidized iron and gneissic iron formations from a stratigraphic log at Sanaga prospect

	Oxidized iron formation				Gneissic iron formations			
Variable	Observations	Minimum	Maximum	Average	Observations	Minimum	Maximum	Average
Al_2O_3	20	1.080	25.400	9.344	14	0.480	8.690	3.069
Fe_2O_3	20	6.960	58.540	40.399	14	23.320	55.400	44.602
SiO_2	20	27.600	65.800	44.025	14	41.900	59.100	47.943
K_2O	20	0.001	2.520	0.260	14	0.017	2.000	0.536
MgO	20	0.020	1.290	0.190	14	0.630	2.930	1.889
MnO	20	0.009	0.137	0.035	14	0.049	0.091	0.066
Na_2O	20	0.005	0.070	0.040	14	0.070	2.260	0.596
CaO	20	0.005	0.830	0.072	14	0.870	3.880	1.568
TiO_2	20	0.060	2.050	0.489	14	0.040	0.360	0.186
Cr_2O_3	20	0.001	0.017	0.006	14	0.001	0.011	0.004
P_2O_5	20	0.026	0.289	0.079	14	0.040	0.072	0.052
LOI	20	0.380	14.540	4.766	14	-1.390	1.660	-0.739

Table 4. Trace elements (ppm) geochemistry of a diamond drill in the Sanaga prospect.

Lithotypes	From	To	Sample	Ni	Pb	Sn	As	Ba	Cl	Co	Cu	Sr	V	Zn	Zr	Co/Zn
Oxidized cap	0.80	1.15	106703	2.00	5.00	0.10	1.00	1.00	2.00	0.10	8.00	2.00	5.00	12.00	18.00	0.01
	1.15	1.80	106704	5.00	6.00	1.00	1.00	4.00	3.00	0.10	5.00	3.00	5.00	8.00	22.00	0.01
	1.80	2.95	106705	13.00	7.00	2.00	0.10	3.00	5.00	1.00	5.00	3.00	4.00	7.00	11.00	0.14
	2.95	3.75	106706	15.00	6.00	1.00	1.00	3.00	2.00	0.10	2.00	2.00	2.00	5.00	7.00	0.02
	3.75	4.25	106708	6.00	6.00	1.00	1.00	0.10	2.00	0.10	0.10	3.00	2.00	4.00	7.00	0.03
Oxidized gneiss	4.25	5.70	106709	1.00	5.00	1.00	1.00	1.00	2.00	0.10	0.10	3.00	7.00	6.00	15.00	0.02
	5.70	6.60	106710	0.10	2.00	0.10	0.10	0.10	0.10	0.10	2.00	1.00	12.00	6.00	24.00	0.02
	6.60	7.80	106711	1.00	6.00	0.10	0.10	5.00	2.00	0.10	2.00	28.00	21.00	4.00	35.00	0.03
	7.80	8.43	106713	2.00	3.00	0.10	1.00	5.00	2.00	0.10	2.00	3.00	20.00	3.00	43.00	0.03
Magnetite gneiss	8.43	8.79	106714	2.00	6.00	1.00	0.10	0.10	4.00	0.10	3.00	2.00	6.00	5.00	13.00	0.02
	8.79	9.43	106715	3.00	6.00	2.00	0.10	2.00	1.00	0.10	6.00	2.00	1.00	3.00	5.00	0.03
	9.43	10.25	106716	0.10	4.00	0.10	1.00	0.10	1.00	0.10	0.10	1.00	1.00	3.00	4.00	0.03
	10.25	11.77	106717	0.10	0.10	0.10	1.00	0.10	1.00	0.10	0.10	0.10	0.10	2.00	4.00	0.05
	11.77	13.00	106718	1.00	6.00	2.00	0.10	0.10	2.00	0.10	2.00	2.00	2.00	3.00	4.00	0.03
	13.00	14.60	106719	0.10	2.00	0.10	1.00	0.10	1.00	0.10	0.10	1.00	1.00	2.00	3.00	0.05
	14.60	15.58	106720	2.00	5.00	0.10	0.10	10.00	0.10	0.10	0.10	0.10	3.00	3.00	13.00	0.03
	15.58	16.25	106721	0.10	2.00	1.00	0.10	10.00	3.00	0.10	0.10	0.10	0.10	2.00	24.00	0.05
	16.25	17.83	106723	0.10	4.00	0.10	0.10	13.00	2.00	0.10	1.00	1.00	1.00	3.00	7.00	0.03
	17.83	19.25	106724	2.00	3.00	1.00	0.10	91.00	5.00	0.10	1.00	4.00	1.00	6.00	21.00	0.02
Magnetite amphibole gneiss	19.25	20.82	106725	4.00	6.00	1.00	0.10	83.00	15.00	1.00	3.00	11.00	7.00	10.00	21.00	0.10
	20.82	22.25	106726	9.00	7.00	2.00	1.00	27.00	8.00	0.10	1.00	63.00	3.00	6.00	15.00	0.02
	22.25	24.00	106728	2.00	0.10	2.00	1.00	60.00	9.00	0.10	1.00	17.00	2.00	5.00	11.00	0.02
	24.00	27.00	106731C	3.00	1.00	2.00	0.10	60.00	16.00	0.10	2.00	17.00	4.00	5.00	8.00	0.02
	27.00	30.00	106735C	3.00	0.10	1.00	2.00	13.00	13.00	0.10	2.00	3.00	2.00	5.00	4.00	0.02
	30.00	33.00	106738C	5.00	1.00	1.00	1.00	42.00	35.00	1.00	2.00	12.00	10.00	6.00	7.00	0.17
Enrich magnetite amphibole gneiss	33.00	36.00	106741C	3.00	1.00	0.10	2.00	5.00	7.00	0.10	3.00	3.00	1.00	5.00	4.00	0.02
	36.00	40.00	106746C	4.00	4.00	2.00	1.00	5.00	7.00	0.10	2.00	3.00	2.00	5.00	6.00	0.02
	40.00	44.00	106751C	3.00	5.00	2.00	1.00	40.00	7.00	0.10	3.00	11.00	2.00	6.00	10.00	0.02
	44.00	47.00	106755C	6.00	1.00	2.00	1.00	0.10	2.00	0.10	2.00	2.00	1.00	3.00	4.00	0.03
	47.00	50.00	106758C	1.00	0.10	0.10	2.00	2.00	4.00	0.10	2.00	0.10	1.00	2.00	2.00	0.05
	50.00	53.00	106761C	4.00	0.10	0.10	1.00	1.00	5.00	0.10	3.00	1.00	1.00	3.00	4.00	0.03
	53.00	56.00	106765C	0.01	0.00	0.00	0.00	0.00	0.01	0.00	0.00	0.00	0.01	0.01	0.01	0.20
	56.00	58.00	106768C	0.01	0.00	0.00	0.00	0.02	0.01	0.00	0.00	0.01	0.01	0.01	0.01	0.20
	58.00	59.24	106769	0.00	0.00	0.00	0.00	0.01	0.01	0.00	0.00	0.00	0.00	0.01	0.01	0.11

Table 5. Linear inter-element correlations of oxidize carp iron mineralisation (n=20)

	Al_2O_3	Fe_2O_3	SiO_2	K_2O	MgO	MnO	Na_2O	CaO	TiO_2	Cr_2O_3	P_2O_5	LOI	S	Ni	Pb	Sn	As	Ba	Cl	Co	Cu	Sr	V	Zn	Zr
Al_2O_3	1,00																								
Fe_2O_3	-0,86	1,00																							
SiO_2	0,27	-0,71	1,00																						
K_2O	0,33	-0,60	0,66	1,00																					
MgO	0,21	-0,46	0,54	0,72	1,00																				
MnO	-0,03	-0,21	0,42	0,52	0,79	1,00																			
Na_2O	0,02	-0,24	0,44	0,27	-0,06	-0,03	1,00																		
CaO	0,40	-0,23	-0,14	-0,01	0,18	-0,03	-0,51	1,00																	
TiO_2	0,76	-0,40	-0,32	-0,05	0,01	-0,18	-0,23	0,56	1,00																
Cr_2O_3	0,43	-0,02	-0,54	-0,21	-0,25	-0,24	-0,47	0,44	0,73	1,00															
P_2O_5	0,66	-0,27	-0,43	-0,12	-0,04	-0,21	-0,24	0,54	0,98	0,69	1,00														
LOI	0,95	-0,69	0,00	0,13	0,05	-0,17	-0,11	0,43	0,89	0,59	0,82	1,00													
S	0,62	-0,18	-0,51	-0,27	-0,36	-0,44	-0,24	0,37	0,88	0,83	0,86	0,80	1,00												
Ni	-0,33	0,39	-0,26	-0,08	-0,11	0,08	-0,23	-0,14	-0,19	0,42	-0,17	-0,30	-0,06	1,00											
Pb	-0,20	0,35	-0,34	-0,13	-0,08	0,25	-0,36	0,12	-0,01	0,35	0,05	-0,15	0,06	0,56	1,00										
Sn	-0,39	0,28	0,02	0,07	-0,01	0,12	0,04	-0,26	-0,35	-0,09	-0,30	-0,41	-0,29	0,47	0,57	1,00									
As	-0,38	0,57	-0,57	-0,36	-0,29	-0,31	-0,10	-0,16	-0,08	0,10	-0,05	-0,25	0,09	0,11	-0,19	-0,33	1,00								
Ba	0,29	-0,54	0,59	0,95	0,86	0,72	0,15	0,04	0,00	-0,16	-0,05	0,11	-0,28	-0,01	-0,02	0,10	-0,36	1,00							
Cl	0,10	-0,22	0,25	0,55	0,83	0,78	-0,23	0,09	0,06	0,00	0,06	0,02	-0,21	0,21	0,30	0,29	-0,29	0,75	1,00						
Co	-0,07	0,02	0,06	0,22	0,52	0,58	-0,44	0,04	-0,01	0,13	-0,03	-0,10	-0,17	0,46	0,36	0,38	-0,30	0,41	0,78	1,00					
Cu	-0,15	0,32	-0,41	-0,12	-0,10	0,01	-0,56	-0,05	0,05	0,32	0,11	-0,01	0,16	0,31	0,49	0,34	-0,08	-0,05	0,18	0,28	1,00				
Sr	0,48	-0,28	-0,14	0,13	0,24	0,10	-0,47	0,92	0,64	0,56	0,62	0,50	0,44	-0,02	0,32	-0,10	-0,24	0,21	0,29	0,19	0,08	1,00			
V	0,69	-0,29	-0,43	-0,13	-0,06	-0,19	-0,30	0,57	0,99	0,80	0,97	0,84	0,91	-0,10	0,09	-0,31	-0,04	-0,07	0,04	0,02	0,12	0,65	1,00		
Zn	0,01	0,09	-0,19	0,24	0,27	0,38	-0,52	-0,05	0,07	0,37	0,06	0,06	0,16	0,29	0,41	0,10	0,05	0,35	0,53	0,46	0,67	0,16	0,14	1,00	
Zr	0,86	-0,58	-0,09	0,20	0,12	-0,07	-0,20	0,36	0,87	0,65	0,82	0,92	0,78	-0,14	-0,07	-0,27	-0,12	0,22	0,19	0,03	0,12	0,49	0,83	0,24	1,00

Table. 6. Linear inter-element correlations of magnetite gneiss and magnetite amphibolite gneiss (n=14)

	Al_2O_3	Fe_2O_3	SiO_2	K_2O	MgO	MnO	Na_2O	CaO	TiO_2	Cr_2O_3	P_2O_5	LOI	S	Ni	Pb	Sn	As	Ba	Cl	Co	Cu	Sr	V	Zn	Zr
Al_2O_3	1,00																								
Fe_2O_3	-0,99	1,00																							
SiO_2	0,97	-0,98	1,00																						
K2O	0,86	-0,87	0,89	1,00																					
MgO	-0,34	0,32	-0,46	-0,27	1,00																				
MnO	0,28	-0,25	0,15	-0,10	0,21	1,00																			
Na2O	0,89	-0,89	0,85	0,93	0,01	0,12	1,00																		
CaO	0,64	-0,62	0,50	0,24	0,16	0,79	0,50	1,00																	
TiO_2	0,59	-0,57	0,49	0,41	0,11	0,65	0,52	0,73	1,00																
Cr_2O_3	0,53	-0,48	0,44	0,15	-0,32	0,57	0,24	0,69	0,52	1,00															
P_2O_5	0,14	-0,12	0,19	-0,07	-0,64	0,38	-0,23	0,11	0,29	0,41	1,00														
LOI	0,85	-0,82	0,84	0,54	-0,62	0,44	0,51	0,63	0,56	0,75	0,56	1,00													
S	0,58	-0,55	0,43	0,51	0,42	0,37	0,73	0,64	0,57	0,18	-0,44	0,24	1,00												
Ni	0,37	-0,34	0,34	0,02	-0,46	0,21	0,08	0,41	-0,11	0,70	0,17	0,57	0,03	1,00											
Pb	0,31	-0,26	0,33	0,06	-0,59	0,22	0,00	0,24	0,05	0,58	0,32	0,60	-0,05	0,68	1,00										
Sn	0,54	-0,49	0,54	0,52	-0,52	-0,13	0,43	0,06	-0,05	0,42	0,03	0,51	0,20	0,61	0,61	1,00									
As	-0,23	0,21	-0,19	-0,29	-0,14	-0,38	-0,31	-0,20	-0,64	-0,32	-0,17	-0,17	-0,20	0,30	0,08	0,04	1,00								
Ba	0,89	-0,89	0,89	0,94	-0,31	-0,05	0,91	0,34	0,36	0,22	-0,12	0,61	0,62	0,22	0,23	0,64	-0,08	1,00							
Cl	0,61	-0,61	0,52	0,44	0,27	0,33	0,68	0,68	0,29	0,20	-0,40	0,33	0,80	0,37	0,07	0,29	0,20	0,61	1,00						
Co	0,40	-0,38	0,24	0,16	0,48	0,46	0,48	0,74	0,33	0,26	-0,47	0,18	0,85	0,32	0,00	0,09	0,14	0,36	0,90	1,00					
Cu	-0,07	0,06	-0,02	-0,01	-0,05	-0,49	0,01	-0,21	-0,68	-0,24	-0,59	-0,22	-0,02	0,40	0,20	0,25	0,66	0,15	0,33	0,23	1,00				
Sr	0,71	-0,68	0,72	0,37	-0,72	0,37	0,32	0,54	0,37	0,77	0,60	0,96	0,06	0,71	0,73	0,53	0,00	0,47	0,23	0,09	-0,08	1,00			
V	0,65	-0,64	0,53	0,42	0,26	0,44	0,68	0,78	0,37	0,37	-0,36	0,42	0,84	0,45	0,18	0,34	0,09	0,60	0,97	0,93	0,26	0,32	1,00		
Zn	0,53	-0,51	0,55	0,41	-0,40	-0,12	0,42	0,24	-0,14	0,23	-0,17	0,46	0,32	0,69	0,57	0,71	0,50	0,65	0,65	0,43	0,65	0,52	0,62	1,00	
Zr	0,74	-0,70	0,76	0,56	-0,71	0,01	0,47	0,32	0,13	0,53	0,20	0,80	0,25	0,72	0,73	0,79	0,18	0,73	0,40	0,21	0,30	0,83	0,45	0,83	1,00

Oxidized formations are more depleted in trace elements than gneissic. The latter is slightly enrich in Cl, Sr, and Ba, while the former has higher contents in Zr and V.

4.2.3. Linear Inter-element Correlations

Mineral Inter-element correlations matrix of the oxidized cap and gneissic formations are given in Table 5 and Table 6 respectively. Besides correlation characteristic similar in the two formations of the lithological sequence (e.g., Al_2O_3 with LOI ($r > 0.8$), and Zr ($r > 0.7$); LOI with Zr ($r > 0.8$), and S with V ($r > 0.8$)), there are significant correlations specific for the oxidized formations (e.g., Al_2O_3 and TiO_2 ($r > 0.7$); MgO with MnO ($r > 0.7$), Ba ($r > 0.8$), and Cl ($r > 0.8$); TiO_2 with P_2O_5 ($r > 0.9$), LOI (r > 0.8), Cr (r > 0.7), S (r > 0.8), V (r > 0.9), and Zr (r > 0.8); LOI with S (r > 0.7), and V (r > 0.8); and S with Zr (r > 0.7)), and the gneissic formations (e.g., Al_2O_3 with SiO_2 (r > 0.9), Na_2O (r > 0.8), Ba (r > 0.8), K_2O (r > 0.8) and Sr (r > 0.7); SiO_2 with Na_2O (r > 0.8), Ba (r > 0.8), K_2O (r > 0.8) and Sr (r > 0.7); CaO with TiO_2 (r > 0.7), and MnO (r > 0.7)). These correlation are indicative of a terrigenous contribution during the BIF deposition [17,29,30]. The significant positive correlation between Al_2O_3 and TiO_2 (r > 0.7) could be inherent from the common association of Ti and Al in clay minerals from residual weathering.

Beside this positive correlation there is a negative correlation between SiO_2 and Fe_2O_3 (r > 0.5 in both sequences), suggesting the incorporation of Fe_2O_3 and SiO_2 in different mineral phases and inversely reflected the variation of one component to another.

5. Discussion

5.1. Iron Bering Rocks

Many iron occurences are found within the upper Nyong serie in the Ntem complex. Ore bearing rock varies from BIF Koumbo and Elom area to gneissic formations at Ngovayang [3,4,27]. Iron bearing mineralisation from macroscopic description showed that the mineralisation in the Sanaga prospect is carried by magnetite and magnetite amphibolite gneiss. This is in accordance with data obtained by [27]. This fact could permit a bigger comparison in their genesis. However, detail petrographic data are currently prepared for a clear comparison between the Sanaga iron formations and those of the Ngovayang ridge.

5.2. Source of Alumina in the Oxidized Formations

Al_2O_3 is enriched at the top of the sequence compared to bottom. Enrichment in alumina has been considered to result from three main sources: (a) immobile behaviour and residual enrichment of Al_2O_3, (b) introduction of Al_2O_3 during the ore-forming event; (3) introduction of Al_2O_3 during geological recent chemical weathering processes, possibly from adjacent shale unit [31]. Simple residual enrichment of alumina would necessitate very considerable removal of iron during ore formation, rather than it effective residual enrichment as observed elsewhere [32]. There is no considerable removal of Fe_2O_3 at the top profile in the oxidized formation when compared to the gneissic formation, and the concentration of Al_2O_3 (average 9.34 %) instead suggest it introduction during recent chemical weathering. The high LOI obtained (with a maximum of 14.54, Table 2) is in favour of the conclusion.

5.3. Clastic input

Elevated Al_2O_3 and TiO_2 are often type to be indicator of detrital input in iron formations [33]. Likewise, elevated Al_2O_3 and TiO_2 MgO, CaO and K_2O are regularly present in sediments. The geochemical sequences of gneissic formations showed a relatively high amount of Al_2O_3 MgO and TiO_2 ranging between 0.48 – 8.69 %, and 0.04-2.05 % respectively. Equally MgO (0.63 – 2.93 %), CaO (0.87 – 3.88 %), K_2O (0.01 – 2.50 %) and Na_2O (0.07 – 2.26 %) showed an increase. Al_2O_3 and TiO_2 are generally used to trace clastic input [28,34]. It has been suggested that, high content of Al_2O_3 together with high amounts of TiO_2 are evidence of the supply of primary materials from deeply weathered source rocks [35]. The incorporation of terrigenous sediments in gneissic formations of the Sanaga prospect is suggested by the strong correlation between Al_2O_3 with TiO_2, and Zr, (Table 4), as Zr is an element considered as a detrital component [36]. The relatively low content of these elements indicated a low degree of contamination [17].

5.4. Source of Fe and Si

Even with the huge amount of data concerning the origin of Fe and Si in iron formations, controversies remain very high. The majority of writers agree that iron formations are chemical sediments formed by precipitation of iron and silica from solutions consisting of a mixture of seawater with hydrothermal fluids. The main impurities are terrigenous sediments carried by rivers or winds, or deposited by volcanic activity [37,38,39]; or pelagic sediments [40]. Most workers consider that Fe and Si components are derived from the leaching of basalt and komatiites of the ocean floor by hydrothermal fluids [12,29,41,42,43]. Only a few authors attribute the origin of Fe and Si to the weathering of continental rocks [44,45,46]. Proposed methods for distinguishing between seawater, hydrothermal, biogenic and detrital sources are based on differences in the mineralogical, chemical and isotopic composition.

Again [47] suggested that hydrothermal metal-rich deposits could be distinguished from hydrogenous deposits formed by diagenetic processes on the basis of the relative abundance of SiO_2 and Al_2O_3. Due to the fact that the top sequences were weathered, data plots were taken for the gneissic formation from 20 m depth in fresh samples. SiO_2 and Al_2O_3 diagram (Figure 3) plotting of study samples showed that, they fall into the hydrothermal and hydrogenous zone. Pure hydrothermal deposits contain very little Al and have high Al/Ti ratios [48]. Contamination of such deposits by pelagic and terrigenous deep-sea sediments enriches them in components such as Ti and Al, resulting drastic lowering of the Fe/Ti ratios and increase in the Al/(Al + Fe + Mn) ratio. On an Fe/Ti vs. Al/(Al + Fe + Mn) diagram of [49] , most of the studied core samples cluster on the East Pacific Rise hydrothermal deposits (Figure 4). Furthermore, the Si/Al ratio is commonly used to detect eventual hydrogenous, respectively hydrothermal material supply. It is worth underlining here that the Si/Al ratio has been used to distinguish between hydrothermal Fe–Mn crusts, rich in Si and characterized by a Si/Al ratio >5.1, and hydrogeneous Fe-deposits (nodules), whose typical Si/Al ratio is 3, the same as marine sediments. The average Si/Al ratio of the studied iron formation is 21.17 pointing to the hydrothermal origin of the studied iron formation (Table 2).

However, some samples fall into the hydrogenous field (Figure 3) suggesting chemical precipitation from seawater [50]. The seawater is equally suggested by the low CaO/(CaO+MgO) ration (between 0.17 – 0.70) indicative of sediments that precipitated from seawater.

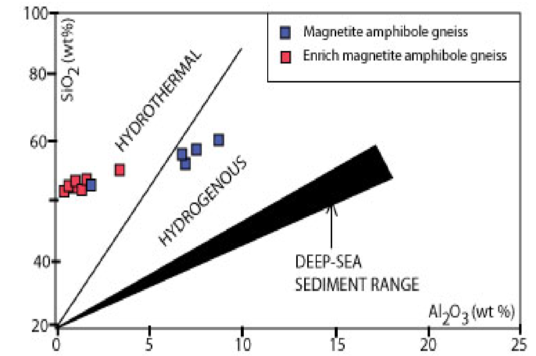

Figure 3. Plot of Al_2O_3 Vs SiO_2 discrimination diagram indicating the hydrothermal and hydrogenous affinity of the studied gneiss

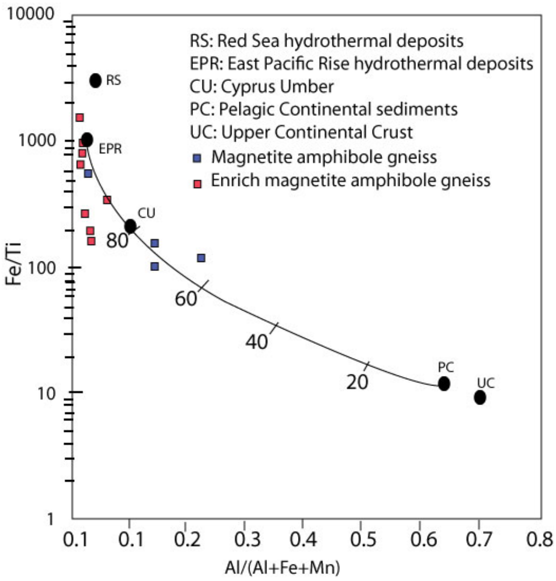

Figure 4. Fe/Ti vs. Al/(Al + Fe + Mn) diagram of the Sanaga gneissic formations compared to the East Pacific Rise hydrothermal deposits and Cyprus Umber (adopted from [54])

Additionally, it is known that Co/Zn ratio is used as tracer of hydrothermal origin [56]. According to this author, low Co/Zn ratio (0.15) characterizes hydrothermal deposits whereas hydrogenous deposits display high Co/Zn ratio (2.5). The average Co/Zn ratio of the studied iron ores samples is 0.04, which is consistent with trace metals derived from a largely hydrothermal source [51].

5.5. Iron Potential

Major elements diagram plotted of the Sanaga iron formations with that of average Agloma and Lake Superior showed a similar mineralogy with a slight enrichment of iron and silica at from ore of the Sanaga prospect (Figure 5). This diagram shows that the ore have an interesting potential for exploitation.

The potential of iron ore mineralisation is generally viewed using the iron percentage, the deleterious elements encountered such as P_2O_5 and S, Al_2O_3, and SiO_2. The deleterious effects of such elements in the production process and metallurgical properties of steel have long been recognized [52,53]. For that reason [54] divided iron ore in three main category base on the Fe percentage: (1) high grade iron ores with iron percentage > than 65 %, (2) average grade with iron ranging between 65<Fe %>52, (3) low grade with Fe< 52 %. Based on this classification it is clear that the iron mineralisation of the Sanaga prospect is of low grade (average Fe is 40.94 wt %) but largely remain in the extracting range since the Fe_2O_3 percentage vary between 27.55 – 58.54 wt % for the oxidized iron formation and 23.32 – 55.40 wt % for gneissic formations. The total gangue content (Al_2O_3 and SiO_2 represent the main gangue in the composition of this iron formation with an average of 53.36 wt % and 51.00 wt % in the oxidized and gneissic formation respectively. This total result combine with total iron percentage showed that the Sanaga iron formations are of low grade.

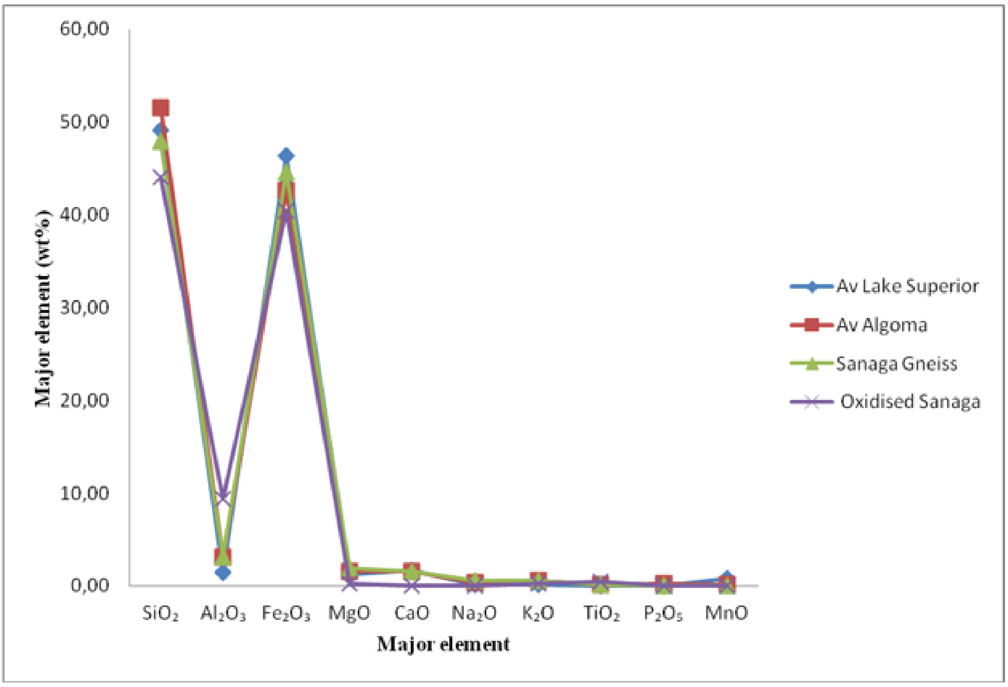

Figure 5. Major elements of a drill hole from the Sanaga prospect compared with the Algoma and Lake Superior types iron formation

Silicon and Al also impact greatly on the toughness and ductility of cast and deformed steel [55]. Consequently, understanding and defining the mineralogical association of such deleterious elements is critical in developing strategies on how to best manage and process high-grade ore.

Phosphorous and sulfur represent contamination in steel making process and are among the main target during drilling and iron ore beneficiation. As example, for all the elements commonly present in steel, phosphorus has the most embrittling effect [55], the degree of which can be enhanced by the presence of other alloying elements in steel, particularly Cr and Mn [56]. The present bulk of production is a blend of low P <0.07 % [57]. Average P value in the Sanga permit is exactly 0.07 %. Again, sulphur content in both oxidized and gneissic formations from Sanaga is very low, below the acceptable 0.1 % in steel making [58,59]. This two deleterious elements values are within the acceptable ranges, making the ore suitable for the production of steel.

6. Conclusions and Perspectives

The current study highlights a number of common feature in the Sanaga prospect base on drill hole chemical data, and the following conclusions could be derived:

(1) Iron ore mineralisation of the Sanaga prospect is hosted by magnetite gneiss similar to that observed in the Ngovayang ridge located in the Nyong Unit.

(2) The high concentration of Al_2O_3 (average 9.34 %) in the oxidized iron formations is due to recent chemical weathering.

(3) Major elements with the couple SiO_2/ Al_2O_3 and Si/Al ratio as well as trace metals ratio average (Co/Zn) confirm the hydrothermal nature of Fe and Si.

(4) The Sanaga iron formations are metamorphose chemical sediments formed by precipitation of iron and silica from a mixture of seawater and hydrothermal fluids with a minor terrigenous input.

(5) P_2O_5 as well as Sulphur percentage are very low making the iron ore suitable for the production of steel.

The low suite of trace elements from the deposit did not permit to increase geochemical evidence regarding the origin of this iron prospect. For the better understanding of the deposit, feature work would be very important. In this, the development of polished thin section, scan electron microscopy, full suite of geochemical analyses, and effective dating of this iron formation to study the various iron oxide, develop a model of iron formation and determinate the various mineral phases bearing some of the deleterious elements could be envisaged. Additionally a detail petrology is required to increase knowledge in the prospect.

Acknowledgements

We gratefully acknowledge the assistance of the Cameroun Mining Company (CMC) for making available the geochemical data and drill core of a hole within their Sanaga permit.

References

[1] Teutsong T., Bontognali T. R. R., Ndjigui P-D., Vrijmoed J. C., Teagle D., Cooper M., Vance D., Petrography and geochemistry of the Mesoarchean Bikoula banded iron formation in the Ntem complex (Congo craton), Southern Cameroon: Implications for its origin, *Ore. Geol. Rev.* 80, 267-288, 2017.

[2] Ndong B.F., Sobdjou K.C., Yannah M., Ntomba M. S., Nzenti J. P., Mvondo O. J., Origin and tectonic framework of the Ngovayang Iron Massifs, southern Cameroon. *Sci. Res.* 4, 11-20, 2016.

[3] Ganno, S., Ngnotue, T., Kouankap, N.G.D., Nzenti, J.P., Notsa, F.M., Petrology and geochemistry of the banded iron-formations from Ntem complex greenstones belt, Elom area, Southern Cameroon: implications for the origin and depositional environment. *Chem. Erde 75*, 3, 75-387, 2015a.

[4] Ganno, S., Moudioh, C., Nzina Nchare, A., Kouankap Nono, G.D., Nzenti, J.P., Geochemical fingerprint and iron or epotential of the siliceous itabirite from Palaeoproterozoic Nyong series, Zambi area, Southwestern Cameroon. *Res. Geol*. 66 (1), 71-80, 2015b.

[5] Ganno S, Njiosseu T.E.L., Kouankap Nono G.D., Djoukouo S.A., Moudioh C., Ngnotue T., Nzenti, J.P., A mixed seawater ad hydrothermal origin of the superior-type banded iron formation (BIF)-hosted Kouambo iron deposit, Palaeoproterozoic Nyong series, Southwestern Cameroon: Constraints from petrology and geochemistry, *Ore. Geo. Rev. 80*, 860-875, 2016.

[6] Ilouga D.C.I., Suh, C.E., Ghogomu R.T., Textures and rare earth elements composition of banded iron formations (BIF) at Njweng prospect, Mbalam Iron Ore District, Southern Cameroon. *Int. Jour. Geo.*, 4, 146-165, 2013.

[7] Kock M.O., Evans A.D., Gutzmer J., Beukes J., Dorland H. C., Origin and timing of banded iron formation-hosted high-grade hard hematite Deposits- A paleomagnetic approach. *Econ. Geol. Rev., 15*, 49-71, 2008.

[8] Mukhobaday J., Gtzmer J., Beukes N.J., Bhattacharya H. N., Geology and genesis of the major banded iron formation-hosted high-grade iron ore deposits of India, *Econ. Geol. Rev. 15*, 291-315, 2008.

[9] Beukes, N.J., Gutzmer, J., Origin and paleoenvironmental significance of major iron formations at the Archean-Paleoprotorozoic boundary, *Econ. Geol. Rev.*, 15, 5-47, 2008.

[10] Gutzmer, J., Beukes, N.J., de Kock, M. O., and Netshiozwi, S. T., Origin of high-grade iron ores at the Thabazimbi deposit, South Africa: Iron Ore Conference, *Fremantle, 19–21 September 2005*, Proceedings, 57-65, 2005.

[11] Bau, M., and Dulski, P., Distribution of yttrium and rare-earth elements in the Penge and Kuruman iron-formations, Transvaal Supergroup, South Africa. *Precamb. Res., 79*, 37-55, 1996.

[12] Klein, C., and Beukes, N. J., Time distribution, stratigraphy, and sedimentologic setting, and geochemistry of Precambrian iron-formations. In Schopf, J. W., and Klein, C. (eds.), The Proterozoic Biosphere: A Multidisciplinary Study. Cambridge: University of Cambridge, 139-146, 1992.

[13] Pearce, J.A., Gale, G.H., Identification of ore- deposition environment from trace-element geochemistry of associated igneous host rocks. *Geol. Soc. Lon., special publications 7*, 14-24, 1977.

[14] Graf J.L., "Rare Earth Elements as Hydrothermal Tracers during the Formation of Massive Sulfide Deposits in Volcanic Rocks," *Econ. Geol.* Vol. 72, No. 4, 527-548, 1977.

[15] Chen, J., Walter, M.R., Logan, G.A., Hinman, M .C., Summons, R. E., *The paleoproterozoic Mcarthur River (HYC) Pb-Zn-Ag deposit of northen Ausralia*, organic geochemistry and ore genesis. Earth and plan. science Let. 210, 2003, 467-479.

[16] Landis, G.P., Rye, R.O., Characterzation of gas chemistry and noble-gas isotope ratios of inclusion fluids in magmatic-hydrothermal and magmatic-stream alunite, *Chem. Geol, 215*, 155-184, 2005.

[17] Spier, C.A., Oliveira, S.M.B., Sial, A.N., Rios, F.J., Geochemistry and genesis of banded iron formations of the Cauê Formation, quadrilátero Ferrifero, Minas Gerais, Brazil. *Precamb. Res.*, 152, 170-206, 2007.

[18] Viehmann S, Bau M, Smith AJB, Beukes NJ, Dantas EL, Bühn, B., The reliability of ~2.9 Ga old Witwatersrand banded iron formations (South Africa) as archives for Mesoarchean seawater: Evidence from REE and Nd isotope systematic. *J. Afr Earth Sci 111*, 322-334, 2015.

[19] Davy R., A contribution on the chemical composition of Precambrian iron-formations, in Iron formation: Facts and problems (Eds: A. F. Trendall and Morris) *Developments in Precambrian Geology 6*, Elsevier, 211-251 1983.

[20] Toteu S.F., Van Schmus W.R., Penaye J., Nyobé J.B., U-Pb and Sm-Nd evidence for Eburnean and Pan-African highgrade metamorphism in cratonic rocks of southern Cameroon, *Precamb. Res. 67*, 321-347, 1994.

[21] Lerouge C, Cocherie A, Toteu S.F., Penaye J., Milési J.P., Tchameni R., Nsifa E.N., Fanning C.M., Doloule E., Shrimps U-Pb zircon age evidence for Paleoproterozoic sedimentation and 2.05Ga syntectonic plutonism in the Nyong Group, SouthWestern Cameroon: consequences for the Eburnean-Transamazonian belt of NE Brazil and Central Africa. *J Afr Earth Sci*. 44, 413-427, 2006.

[22] Shang C.K., Satir M., Siebel W., Nsifa E.N., Taubald H., Liegeois J.P., Tchoua F.M., TTG magmatism in the Congo craton; a view from major and trace element geochemistry, Rb–Sr and Sm–Nd systematics of TTG magmatism in the Congo craton: case of the Sangmelima region, Ntem complex, southern Cameroon. *J Afr Earth Sci 40*: 61-79, 2004a.

[23] Shang C.K., Satir M., Nsifa E.N., Liegeois J.P., Siebel W., Taubald H., Archaean highK granitoids produced by remelting of the earlier Tonalite–Trondhjemite–Granodiorite (TTG) in the Sangmelima region of the Ntem complex of the Congo craton, southern Cameroon. Int J Earth Sci 96: 817-842, 2007.

[24] Ebah Abeng, S.A.E., Ndjigui, P.D., Beyanu, A.A., Teutsong, T., Bilong. P., Geochemistry of pyroxenites, amphibolites and their weathered products in the Nyong unit, SW Cameroon (NW border of Congo Craton): Implications for Au-PGE exploration. *Journal of Geochem. Expl, 114*, 1-19, 2012.

[25] Chombong N.N., Suh C.E., 2883 Ma commencement of BIF deposition at the northern edge of Congo craton, southern Cameroon: new zircon SHRIMP data constraint from metavolcanics. *Episodes. 36*:47-57, 2013.

[26] Nédélec A., Minyem D., Barbey P., High P-High T anatexis of Archean tonalitic grey gneisses: Eséka migmatites, Cameroun. *Precambr Res. 62*:191-205, 1993.

[27] Chombong N.N., Suh C.E., Lehmann B., Vishiti A., Ilouga D.C., Shemang E.M., Tantoh B.S., and Kedia A.C. Host rock geochemistry, texture and chemical composition of magnetite in iron ore in the Neoarchaean Nyong unit in southern Cameroon, *Appl. Earth Sci.*, 17 p., 2017.

[28] Murray, R.W., Jpnes, D.L., Buchholtz, T.B., Diagenetic formation of bedded chert: evidence from chemistry of the chert-shale couplet. *Geophys. J. R. Astron. Soc. 20*, 271-274, 1992.

[29] Beukes, N.J., Klein, C., Geochemistry and sedimentology of a facies transition – from microbanded to granular iron-formation – in the early Proterozoic Transvaal Supergroup, South Africa, *Precamb. Res. 47*, 99-139, 1990.

[30] Horstmann, U.E., Halbich, I.W., Chemical composition of ¨ banded iron-formations of the Griqualand West Sequence, Northern Cape Province, South Africa, in comparison with other Precambrian iron formations. *Precamb. Res. 72*, 109-145, 1995.

[31] Riddley, M., Evidence for the hydrothermal origin of iron ore, Southern Ridge, Mont Tom Price, Western Australia: *Unpublished B.Sc. Thesis, Nedlands, University of Western Australia*, 93 p., 1999.

[32] Webb A., Dickens G., and Oliver N.H.S., From banded iron-formation to iron ore: Geochemical and mineralogical constraints from across the Hamersley Province, Western Australia; *Chem. Geol.* 197 215-251, 2003.

[33] Hatton, O., Davidson, G., Soldiers Cap Group iron-formations, Mt. Isa Inlier, Australia, as windows into the hydrothermal evolution of a base-metal-bearing Proterozoic rift basin. Australian *J. Earth Sci.* 51, 85-106, 2004.

[34] Lan, T.G., Fan, H.R., Santosh, M., Hu, F.F., Yang, K.F., Liu, Y.S., U–Pb zircon chronology, geochemistry and isotopes of the Changyi banded iron formation in the eastern Shandong Province: constraints on BIF genesis and implications for Paleoproterozoic tectonic evolution of the North China Craton. *Ore Geol. Rev. 56*, 472-486, 2014.

[35] Harder, H., Können Eisensäuerlinge die Genese der Lahn-Dill-Erze erklären: *Beiträge zur Mineralogie und Petrographie, v. 9*, p. 379-422, 1964.

[36] Hirst, D.M., The geochemistry of modern sediments from the Golf of Paria, 2. The location and distribution of trace elements. *Geochim. Cosmochim. Acta, 26*:1147-1187, 1962.

[37] Kimberley, M.M., Exhalative origins of iron formations. *Ore Geol. Rev. 5*, 13-145, 1989.

[38] Klein, C., Beukes, N.J., Geochemistry and sedimentary of a facies transition from limestone to iron formation deposition in the Early Proterozoic Transvaal Supergroup, South Africa, *Econ. Geol. 84*, 1733-1774, 1989.

[39] Isley, A.E., Hydrothermal plumes and the delivery of iron to banded iron formation. *J. Geol. 103*, 169-185, 1995.

[40] Lascelles, D.F., Black smokers and the Archean environment: uniformitarian model for the genesis of iron-formations. *Ore Geol. Rev. 32*, 381-411, 2007.

[41] Dymek, R.F., Klein, C., Chemistry, petrology and origin of banded iron-formation lithologies from the 3800 Ma Isua supracrustal belt West Greenland. *Precamb. Res. 39*, 247-302, 1988.

[42] Shimizu, H., Umemotto, N., Masuda, A., Appel, P.W.U., Sources of iron-formations in the Archean Isua and Malene supracrustals West Greenland: evidence from La-Ce and Sm-Nd isotopic data and REE abundances. *Geochim. Cosmochim. Acta 54*, 1147-1154, 1990.

[43] Bau, M., Möller, P., Rare earth element systematics of the chemically precipitated component in Early Precambrian iron-formations and the evolution of the terrestrial atmosphere–hydrosphere–lithosphere system. *Geochim. Cosmochim. Acta 57*, 2239-2249, 1993.

[44] Holland, H.D., The Chemical Evolution of the Atmosphere and the Oceans. *Princeton University Press, Princeton*, 582 pp., 1984.

[45] Manikyamba, C., Balaram, V., Naqvi, S.M., Geochemical signatures of polygenetic origin of the banded iron formation (BIF) of Archean Sandur greenstone belt (schist belt), Karnataka nucleus, India, *Precamb. Res. 61*, 137-164, 1993.

[46] Kholodov, V.N., Butuzova, G.Y., Problems of iron and phosphorus geochemistry in the Precambrian. Lithol. *Miner. Resour. 36 (4)*, 291-302, 2001.

[47] Bonatti, E., Metallogenesis at oceanic spreading centers. Annu. Rev. *Earth and Planet. Sci. 3*, 401-433, 1975.

[48] Marchig, V., Gundlach, H., Möller, P., Schley, F., Some geochemical indicators for discrimination between diagenetic and hydrothermal metalliferous sediments. *Mar. Geol. 50*, 241-256, 1982.

[49] Barrett, T.J., Chemistry and mineralogy of Jurassic bedded chert overlying ophiolites in the North Appenines, Italy. *Chem. Geol. 34*, 289-317, 1981.

[50] Dasgupta, H.C., Sambasiva Rao, V.V., Krishna, C., Chemical environments of deposition of ancient iron- and manganese-rich sediments and cherts. *Sediment. Geol.* 125, 83-9, 1999.

[51] Toth, J.R., Deposition of submarine crusts rich in manganese and iron. *Geo. Soc. Am. Bull. 91 (1)*, 44-54, 1980.

[52] Miller, J.R., *Les impuretés des minerais de fer : les ressources mondiales en minerai de fer. Inventaire et évaluation*. Rapport d'un groupe d'experts nommés par le S.G., Département des affaires économiques et sociales, 447 p, 1972.

[53] Ramanaidou, E., Wells, M., Belton, D., Verall, M., Ryan, C., Mineralogical and microchemical methods for the characterization of high-grade iron formation –derived iron ore: *Econ Geol Rev*, 15, 129- 156, 2008.

[54] Belevtsev, Ya.N., Kravchenko, V.M., Kulik, D.A., Belevtsev, R.Ya., Borisenko, V.G., Drozdovskaya, A.A., Epatko, Yu.M., Zankevich, B.A., Kalinichenko, O.A., Koval, V.B., Korzhnev, M.N., Kusheyev, V.V., Lazurenko, V.I., Litvinskaya, M.A., Nikolayenko, V.I., Pirogov, B.I., Prozhogin, L.G., Pikovskiy, E.Sh., Samsonov, V.A., Skvortsov, V.V., Savchenko, L.T., Stebnovskaya, Yu.M., Tereshchenko, S.I., Chaykin, S.I. and Yaroshchuk, M.A., Precambrian banded iron formations of the European part of the USSR. Genesis of Iron-ores. *Naukova Dumka Press, Kiev (IGCP UNESCO Project, No 247 (in Russian))*, 1991.

[55] Dub, V.S., Dub, A.V., and Makarycheva, E.V., Role of impurity and process elements in the formation of structure and properties of the structural steel, *Metal Science and Heat Treatment,* 279-286, 2006.

[56] Brian, C.L., and Messmer, R.P., An electronic model for the effect of alloying elements of the phosphorus induced grain boundary embrittlement of steel, *Acta Metallugica, 30*, 1811-1818, 1982.

[57] Thorne, W.S., Hagemann, S.G., Webb, A., and Clout, J., Banded iron formation-related iron ore deposits of the Hamersley Province, Western Australia; *Econ Geol Rev, 15*, 197-221, 2008.

[58] Guider, J.W., Iron ore beneficiation - key to modern steelmaking, *Miner. Eng. 33*, 410-413, 1981.

[59] Dobbins, M.S., Burnet, G., Production of an iron ore concentrate from the iron-rich fraction of power plant fly ash. *Resour. Conserv. 9*, 231-242, 1982.